Postprint of: Makoś-Chełstowska P., Słupek E., Gębicki J., Deep eutectic solvents – based green absorbents for effective volatile organochlorine compounds removal from biogas, GREEN CHEMISTRY (2021), DOI: 10.1039/D1GC01735G

ARTICLE

# Deep eutectic solvents – based green absorbents for effective volatile organochlorine compounds removal from biogas

Received 00th January 20xx,
Accepted 00th January 20xx

DOI: 10.1039/x0xx00000x

Patrycja Makoś-Chełstowska*[a], Edyta Słupek [a], Jacek Gębicki [a]

Volatile organochlorine compounds (VOXs) presented in biogas can cause many technological and environmental problems. During the combustion of biogas containing VOXs, the corrosion of installation, as well as the formation of toxic by-products (polyhalogenated dioxins and furans) and further emission to the atmosphere, may occur. Therefore, in this study, a new procedure based on physical absorption was developed. In order to meet the requirements of green chemistry and green engineering, new deep eutectic solvents (DESs) composed of natural components were used in the absorption studies. Several physical properties of new DESs were determined, followed by an explanation of the absorbents formation mechanism, by means of spectroscopic analysis, and density functional theory. The most important absorption parameters i.e. type of DES, gas flowrate, kind of matrix gas, temperature, and initial concentrations of VOXs were optimized. The obtained results indicate that DES composed of syringol and levulinic acid in 1:1 molar ratio could absorb VOXs efficiently. In addition, the DES regeneration studies demonstrated that the absorption capacities of DES did not change after ten absorption-desorption cycles. Studies on the absorption mechanisms indicate that the H-bonding and van der Waals interactions are the main driving force for the VOXs removal from biogas.

## Introduction

Currently, biogas production is of growing importance because of its economic and environmental advantages[1–3]. Biogas is a biofuel formed from the decomposition of organic resources and waste in the anaerobic digestion process. The detailed chemical composition depends mostly on the kind of raw materials used in the fermentation process. Typically, biogas contains methane (30-70% v/v) and carbon dioxide (15-30 % v/v), as well as small amounts of other gases i.e. nitrogen, oxygen, water vapour, hydrogen sulfide, ammonia, and numerous volatile organic compounds (VOCs)[4,5].

Nowadays, there is a need to develop an effective and economically advantageous technology of biogas treatment to the parameters of high-methane gas (natural gas and compressed natural gas). The demand results from the introduction of a 2030 Framework for climate and energy in which 27% share of renewable energy consumption, by the European Union (EU)[6]. In addition, the UE parliament plans to increase the energy target to 35% by 2030. To achieve these targets, EU countries must significantly increase biogas production from waste materials and inject it into transmission networks or use it as a transport fuel. In order to introduce biogas into the natural gas network or use it as alternative transport fuels, biogas must be treated to meet certain quality parameters.

Volatile organochlorine compounds (VOXs) are one of the most technologically troublesome groups of chemical compounds in biogas. VOXs are mainly presented in biogas from sewage treatment plants and landfills[7]. The total VOX concentration in the biogas stream is typically in the range of 259 to 1239 mg/m$^3$ [4,8–10]. Typically in biogas stream VOX included 1,1,1-trichloroethan, 1,1-dichloroethane, 1,1-dichloroethene, 1,2-dichloroethane, 1,2-dichloroethene, carbon tetrachloride, chloroform, tetrachloroethylene, tetrachloroethane, dichloromethane, trichloroethene can be identified [4,8,11–13]. They come from the chemicals used for wastewater and water treatment, disposal of solvents and refrigerants, as well as solid wastes i.e. polyvinyl chloride or some types of biomass[14]. During the biogas combustion process, chlorine compounds react with water vapour forming hydrochloric acid, which corrodes the surface in the combustion chamber. In addition, organic chlorinated compounds can lead to the formation of toxic by-products i.e. polyhalogenated dioxins and furans in combustion processes[15]. Uncontrolled emission of VOXs to the atmosphere can lead to the destruction of the ozone layer and can provide to the formation of photochemical smog as well as global warming.

Due to this, the biogas purification step is a necessity to process to protect the engines and environment[16]. There are several technologies dedicated to the removal of VOX from the gas stream i.e. physical absorption, condensation, biofiltration, and adsorption based on activated carbon[17–19]. However, most of these methods require the application of toxic solvents, high running, and capital investment costs, as well as long-time operation. The replacement or development of these techniques is one of the most important challenges of our days

[a] Department of Process Engineering and Chemical Technology, Faculty of Chemistry, Gdansk University of Technology, G. Narutowicza St. 11/12, 80–233 Gdańsk, Poland
E-mail: patrycja.makos@pg.edu.pl
Electronic Supplementary Information (ESI) available. See DOI: 10.1039/x0xx00000x

for the energetic industry. Physical absorption is considered to be an appropriate method that meets the standards of green technology and engineering, which can have practical use in industry because it can be cheap, effective, and environmentally friendly[20,21]. However, the necessary condition is the selection of an appropriate solvent. The ideal absorbent should be characterized by low viscosity, relatively low toxic, low vapor pressure, high boiling point, high absorption capacity, ease to regenerate, and low cost[22]. One of the solvents that have all these characteristics is water. Water is commonly used in biogas purification processes, mainly for $CO_2$ capture[23–25]. However, due to the fact that the most of the volatile organochlorine compounds are hydrophobic, water is not an appropriate solvent in the absorption process. For hydrophobic components silicone oil,[26] or glycerol, squalene, dinonyl phthalate,[27] poly(N-methylpyrrole), poly(N-methylpyrrole/polystyrenesulfonate),[28] are preferred.

However, some of these solvents are toxic and have not enough sorption capacity. Therefore, alternative "green solvents" are sought to substitute the currently used organic solvents. The first type of well-studied alternative solvents is ionic liquids (ILs) which are salts in the liquid state[29,30]. ILs have unique physicochemical properties that can be tunable through various suitable combinations of cations and ions. Despite the many advantages of ILs application as absorbents including low vapor pressure, hydrophobicity or hydrophilicity, and high absorption capacity, they come with issues like toxicity, poor biodegradability, flammable and expensive preparation, and manufacturing[30–33]. The second type of eco-friendly media utilized as absorbents are Deep Eutectic Solvents (DESs). DESs are eutectic mixtures consisting mainly of two or more compounds in a certain molar ratio. In complex one of the components acts as a hydrogen bond donor (HBD) and the other as a hydrogen bond acceptor (HBA). In consequence, DESs have melting points (MP) lower than the separate components. DESs synthesis is simple, no by-products are formed and do not require further treatment steps and expensive apparatus. DESs have similar physicochemical properties to ILs, but in addition, DESs characterized by non-toxicity, relatively good biodegradability, and possibility to recallability. Such features make DESs widely applied in the separation processes i.e. extraction,[34–38] absorption,[39–44] and adsorption.[45] However, current studies on the application of DESs in gas separations are mainly limited to the removal of inorganic compounds from gas streams i.e. ammonia,[39] carbon dioxide,[46] hydrogen sulfide,[47] water,[48] or sulfur dioxide[49] from air, waste gases or hydrocarbon gases. Only a few works describe volatile organic compounds i.e. sulfides,[43] siloxanes,[22,50] toluene[44,51]. To the best of our knowledge, there are no works dedicated to the removal of volatile organochlorine compounds from the model or real biogas streams using DESs. However, in the future, this approach can lead to creating a pioneering biogas purification technology in which the end product will be high-methane gas which can be directly introduced into transmission networks.

In practice, substances selected for DES synthesis should contain the following groups: -OH, -COOH, -O-$CH_3$, or =O in order to the formation of stable DES structures.[52] Based on the previous studies the most stable DES complexes are formed by strong hydrogen bonds. Other weaker non-bonded interaction have a lower impact on the durability of DES structures in various processes. [53–56] In addition, the active groups of DES should interact with selected impurities, but the interaction should not be too strong to allow desorption of pollutants after the absorption process. However, DESs should not or only slightly absorb methane. It is acceptable to absorb a maximum of 2 % methane [57]. For meet the requirements of the bio-refinery and sustainable development concept, components of DES should come from biomass, fermentation broth, or other readily available sources. [58]

The paper presents the synthesis of new, never-before-published deep eutectic solvents and their use as absorbents for the removal of VOXs from the model biogas stream. Several physical properties of DESs such as viscosity, density, and melting point have been investigated. Molecular characteristics of new DESs were studied by means of Attenuated total reflectance Fourier transform infrared spectroscopy (ATR–FTIR) as well as proton and carbon-13 nuclear magnetic resonance ($^1$H NMR and $^{13}$C NMR). Experimental results were compared with theoretical studies based on density functional theory (DFT). The absorption process was optimized in terms of DES selection, absorption temperature, gas flow, biogas compositions, and initial concentration of VOX. In addition, the possibility of reusability and regeneration of DES were examined. The mechanism of VOX removal from gas streams using DESs was explained by means of DFT and spectroscopic analysis.

## Experimental

### Materials

The following reagents were used in this study: ±camphor (C) with purity ≥ 95%, guaiacol (Gu) with purity ≥ 99%, syringole (Syr) with purity ≥ 98%, levulinic acid (Lev) with purity 97%, 1,1,2,2-tetrachloroethane (TCE) with purity ≥ 98%, 2,2,2-trichloroethanol (TCEtOH) with purity ≥ 99%, dichloromethane (DCM) with purity ≥ 99%, chloroform (CF) with purity ≥ 99%, carbon tetrachloride (TCM) with purity ≥ 99% were purchase from Sigma-Aldrich (USA).
High purity gases i.e. nitrogen (Linde Gas, Poland), air generated by a DK50 compressor with a membrane dryer (Ekkom, Poland), methane (Linde Gas, Poland), and hydrogen generated by Precision Hydrogen 1200 Generator (PEAK Scientific, Scotland, UK), were used for the preparation of biogas and chromatographic analysis.

### Procedures

#### Preparation of DES

DESs were formed by combining ±camphor, guaiacol, syringole, and levulinic acid in a 1:1 mole ratio. DES composed of ±camphor and levulicic acid was mixing in a 1:2 mole ratio. The mixture of DES was stirred magnetically at 60°C until a homogeneous liquid was obtained. The received DESs fluids were then left to cool to room temperature (RT).

**Structural and physicochemical properties of DESs**

In order to the structural analysis of new DESs, the ATR–FTIR spectra were recorded by means of a Bruker Tensor 27 spectrometer (Bruker, USA) with an ATR accessory and OPUS software (Bruker, USA). The following parameters were used: spectral range: 4000 - 600 $cm^{-1}$; resolution: 4.5 $cm^{-1}$; number of sample scans 256; number of background scans 256; slit width 0.5 cm. In addition, NMR spectra of new DESs were prepared in 5 mm tubes by weighing 20 mg of a DES and inserting 0.7 mL of chloroform-d1. The measurements were carried out at 20°C, using Bruker Avance III HD 400 MHz (Bruker, USA).

The melting point (MP) of DESs was determined visually by cooling DESs to -48°C in cryostat (HUBER, Germany), followed by a temperature increase at 1°C/min. The MP was adopted as the temperature at which the first change in the DES aggregate state was observed. The density and viscosity of liquid DESs were measured using 5 mL of absorbents in a temperature range of 25 to 50°C, using BROOKFIELD LVDV-II + viscometer (Labo-Plus, Poland), and DMA 4500M density meter (Anton Paar, Poland).

**Absorption process**

The biogas was prepared by means of the bubbling occurrence. Nitrogen or mixture of gases $CH_4$:$CO_2$:$N_2$:$H_2O$ in various volume ratio was crossed through a vial including 1 mL of all VOXs. The created stream was diluted with nitrogen (or gas mixture) to reach the desired concentration of VOXs in the biogas stream. In the next step, biogas was directed to the column containing DES, in which the absorption process took place based on bubbling. The cleaned biogas stream was directed to the fume hood. The absorption installation used in this work is presented in Fig. 1.

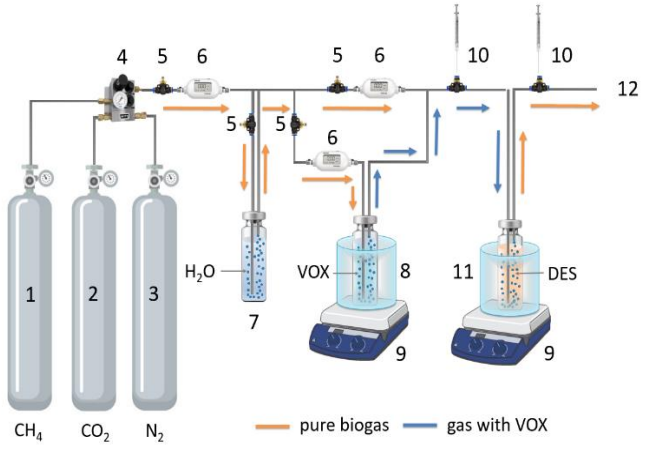


Figure 1 Laboratory absorption installation: 1) bottle with methane; 2) bottle with carbon dioxide; 3) bottle with nitrogen; 4) gas mixer; 5) valve; 6) flowmeter; 7) vial with water; 8) thermostated vial with VOXs; 9) hotplate; 10) gas sample collection point; 11) thermostated vial with DES; 12) gas outlet.

During the absorption process, gas samples were collected before and after the introduction into the absorption column and analyzed by gas chromatography.

The absorption capacity (*q*) was calculated using Equations 1-3, in terms of the mass of selected VOX mass absorbed ($m_{VOX}$) by the mass of DES ($m_{DES}$) used to attain complete saturation ($t_{sat}$):

$$\frac{d(m_{VOX})}{dt} = F \cdot C_{IN} - F \cdot C(t) \quad (1)$$

$$m_{VOX} = F \cdot C_{IN} \cdot \left[t_{sat} - \int_0^{t_{sat}} \frac{C(t)}{C_{IN}} \cdot dt\right] \quad (2)$$

$$q = \frac{m_{VOX}}{m_{DES}} = \frac{F \cdot C_{IN}}{m_{DES}} \cdot \left[t_{sat} - \int_0^{t_{sat}} \frac{C(t)}{C_{IN}} \cdot dt\right] \quad (3)$$

where:
$m_{VOX}$ – VOX mass absorbed [g];
$m_{DES}$ - mass of DES ($m_{DES}$) used to attain complete saturation [g];
$t_{sat}$ – saturation time [min] (time when VOX concentration in the outlet gas is the same as the initial VOX concentration);
$C_{IN}$ – Initial concentration of VOX [g/m³];
*F* – Flow rate of the biogas passing through the absorption column [m³/s];
*C(t)* – concentration of the VOX in outgoing biogas stream measured at intervals during the absorption process [g/m³].

Absorption rate (*N*) was calculated using Equation 4:

$$N = \frac{G_{IN} \cdot Y_{IN} - G_{OUT} \cdot Y_{OUT}}{A} \quad (4)$$

where:
*A* - gas–liquid interfacial area [m²];
$G_{IN}$, $G_{OUT}$ – flow rate [mol/s], which were calculated by determining the volumetric flow rate of mixed gas and the volume percentage of VOX in biogas mixture;
$Y_{IN}$, $Y_{OUT}$ - mole percentage of VOX at inlet, and outlet gas stream.
The gas hold-up ($\varepsilon_G$) was measured using the volume expansion method [59] (Equation 5):

$$\varepsilon_G = \frac{\Delta V}{\Delta V + V_{DES}} \quad (5)$$

ΔV – volume expansion after biogas dispersion [m³];
$V_{DES}$ – Volume of DES in absorption column [m³];

The specific gas–liquid interfacial area (a) was calculated using Equation 6:

$$a = \frac{6 \cdot \varepsilon_G}{d_b \cdot (1 - \varepsilon_G)} \quad (6)$$

where:
$d_b$ – bubble diameter [m].

The gas –liquid interfacial area (A) was calculated using Equation 7:

$$A = a \cdot V_{DES} \quad (7)$$

Absorption processes were carried out until the VOX concentration in the outlet gas was the same as the initial VOX concentration. Each absorption process was repeated three times.

**Chromatographic analysis**

Sample of biogas (0.2 mL) before, during, and after the absorption process was injected into the gas chromatograph Autosystem XL equipped with flame ionization detector (GC-FID) (PerkinElmer, USA), and HP-5 (30 m x 0.25 mm x 0.25 µm) capillary column (Agilent Technologies, USA) in order to determination of VOX in biogas stream. The following chromatographic parameters were used in the study: temperature of oven 60°C, injection port temperature 250°C, injection mode was split 5:1, detector temperature 300°C, the carrier gas - nitrogen (flow rate: 1 mL/min). In addition, the second part of sample (0.5 mL) before, during, and after the absorption process was injected into the gas chromatograph MG#5 (SRI Instruments, USA) equipped with thermal conductivity detector (GC-TCD), and Porapack Q (80/100, 2mm ID) (Restek, USA) packed column in order to studied the concentration of $CO_2$, $N_2$, and $CH_4$ in biogas stream. The following chromatographic parameters were used: temperature of oven 40°C, injection port temperature 60°C, detector temperature 80°C, the carrier gas - helium (flow rate: 5 mL/min). The water concentration in biogas stream was analyzed by means of HIH-4000-002 HONEYWELL sensor.

**Theoretical studies Theoretical studies**

The structures of DESs, VOXs, and DES-VOX complexes were drawn using Avogadro 1.2.0 program.[60] The Orca 4.2.1 software was applied to optimize the geometries of molecules as well as energy interaction between DES and VOX.[61] Gas-phase equilibrium geometries were fully optimized by means of DFT/B3LYP at the 6-311++G** basis set.[62] This level of theory is preferred to investigate the hydrogen bonding in ILs and DESs complexes.[34,49,63,64] The configuration of all ingredients and DESs complexes were inspected to be local minimum by frequency calculations. The interaction energies ($\Delta E_{int}$) of the most stable complexes of all DES-VOX were determined at the B3LYP/6-311++G** level of theory using Equation (8):

$$\Delta E_{int} = E_{DES-VOX} - (E_{DES} + E_{VOX}) \quad (8)$$

where:
$E_{DES-VOX}$ - total energy of DES-VOX complex [kcal/mol];
$E_{DES}$ - total energy of selected DESs [kcal/mol];
$E_{VOX}$ - total energy of selected VOX [kcal/mol].

The $\Delta E_{int}$ was calculated considering the basis set superposition error (BSSE) corrected by means of counterpoise procedure.[65] Non-covalent interaction analysis (NCI) based on Reduced Density Gradient (RDG) was applied in order to explain the nature and strength of the interactions for the studied complexes. The Electrostatic Potential Analysis (ESP) was used to the visualization of relative polarity as well as total charge distribution of the complexes. Both RDG and ESP procedures were made using Multiwfn 3.7 program.[66–68] The graphical representation of the calculated results was made using Gnuplot and Visual Molecular Dynamics 1.9.3.[69] software.

## Results and discussion

**Synthesis and physical properties of DESs**

In the studies, all DESs components, i.e. camphor (C), levulinic acid (Lev), syringol (Syr), and guaiacol (Gu) were blended with each other in a 1:1 molar ratio. However, only mixtures of Syr:Lev (1:1), C:Gu (1:1), Gu:Lev (1:1) were liquids at room temperature (RT). The remaining components were combined in molar ratios of 0.5:1 and 1:2. As a result of further synthesis, an additional liquid complex - C:Lev (1:2) was obtained. The other DESs i.e. C:Lev in 0.5:1 molar ratio, C:Syr in 0.5:1, 1:2 molar ratio, Syr:Gu 0.5:1, 1:2 were solid after cooling to RT.

The melting point (MP) of pure compounds which were used to DESs synthesis i.e. C, Lev, Gu, and Syr equal to 180°C, 33°C, 26°C, and 50°C, respectively. In DESs mixtures meaningful depression of MP with respect to pure compounds was observed. The largest MP depression was observed for C:Gu (1:1) (lower than -48 °C). For the remaining DES, the higher MP were observed which were -43 °C, -23 °C, and +8 °C for Gu:Lev (1:1); Syr:Lev (1:1), and C:Lev (1:2), respectively.

Density ($\rho$) is a typical property for DESs characterization, due to the significant impact on the most of technological processes. DESs densities are strongly dependent on the temperature and exhibit rather higher values than popular organic solvents. In our research, all DESs densities were measured in the temperature range from 293.15 to 323.15 K. The results of the tests are shown in Fig. 2A. All DESs characterized by higher densities than most of the organic solvents, which were 1.0287 ± 0.041, 1.0597 ± 0.052, 1.1382± 0.049, and 1.1675 ± 0.047 g/cm$^3$ for C:Gu (1:1), C:Lev (1:2), Gu:Lev (1:1), and Syr:Lev (1:1) respectively at 20°C. The results presented in Fig. 2A indicates that densities of DESs decrease with temperature increasing. This behavior can be explained by increasing activity and molecular mobility, which provide to increase of solution molar volume, thereby reducing the density.[70]

In the next step viscosity ($\eta$) of liquid DESs was measured in the range of temperature from 293.15 to 323.15 K. Viscosity is an important parameter of solvents in many industrial processes in which fluid flow systems are used. Most of DESs have higher viscosity (>100 cP) compared to water and conventional solvents which can generate problems in the pumping, filtering, or stirring. Therefore, the dynamic viscosity of absorbents (DESs) should be as low as possible. The obtained results indicate that the highest viscosity measurement was attained at 20°C for Syr:Lev (1:1) (31.1 ± 1.2 mPas) followed by Gu:Lev (1:1) (30.0 ± 0.9 mPas), and C:Lev (1:2) (26.2 ± 0.8 mPas). In turn, the lowest viscosity was obtained for C:Gu (1:1) (10.9 ± 0.4 mPas) (Fig. 2B). In addition, similar to the observation of density behavior, the dynamic viscosity is strongly affected by temperature. As the temperature increases, the dynamic viscosity of all new absorbents drastically decreases. This is due to the fact that the temperature increase of DES causes an increase in the average speed of the molecules in the liquid phase which decreases the intermolecular forces. This can reduce the fluid resistance to flow (dynamic viscosity).[71]

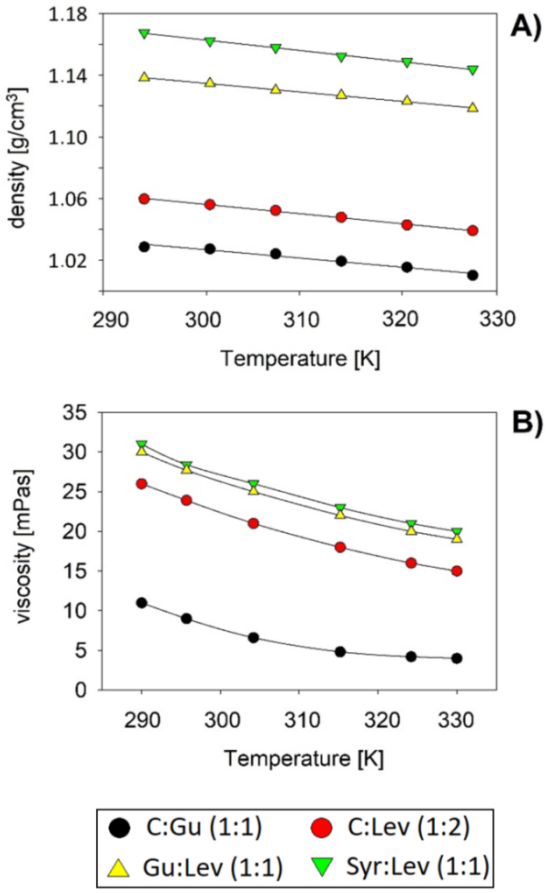


Figure 3 A) Density, and B) viscosity of DESs in range of 293.15 to 323.15 K.

**Structural characterization of DESs formation**

**An experimental studies on DES structural characterization**

In order to experimentally explain the structures of the new DESs, the $^{1}$H NMR and $^{13}$C NMR spectra were recorded (Fig. 3 and Fig. S1–S3). The NMR spectra allow the identification of the atoms of HBA and HBD in DESs structures. The obtained results indicate that only signals from HBA and HBD are visible in the NMR spectra in all of examined DESs. The absence of additional peaks in the NMR spectra confirms that the synthesis reaction proceeded without additional side reactions.

In order to determine the interaction between ingredients in DESs, the proton and carbon chemical shifts (δδ) were calculated. In Syr:Lev (1:1) spectra, the differences among the chemical shift of the proton in the hydroxyl group with connection to pure syringol and with connection to DES were taken into account. The chemical shift value of the proton in the hydroxyl group (-OH) in Syr:Lev (1:1) (δδ H-Syr:Lev = 5.51 ppm) comparison to the chemical shift of the in a pure syringol. (δδ H-Syr = 5.55 ppm) is decreased by 0.04 ppm (Fig. 3). Additionally, the proton chemical shifts influence the carbon chemical shifts (δδ). This effect is confirmed by the formation of a H-bond between the hydroxyl group (-OH) in syringol and the carbonyl group (C=O) in the levulinic acid. Both chemical shifts towards lower values of the carbon atom connected to the OH group with relative to pure syringol (δδ = 0.21 ppm) and the carbon atom from the C=O group with relative to pure levulinic acid (δδ = 0.80 ppm) were observed.

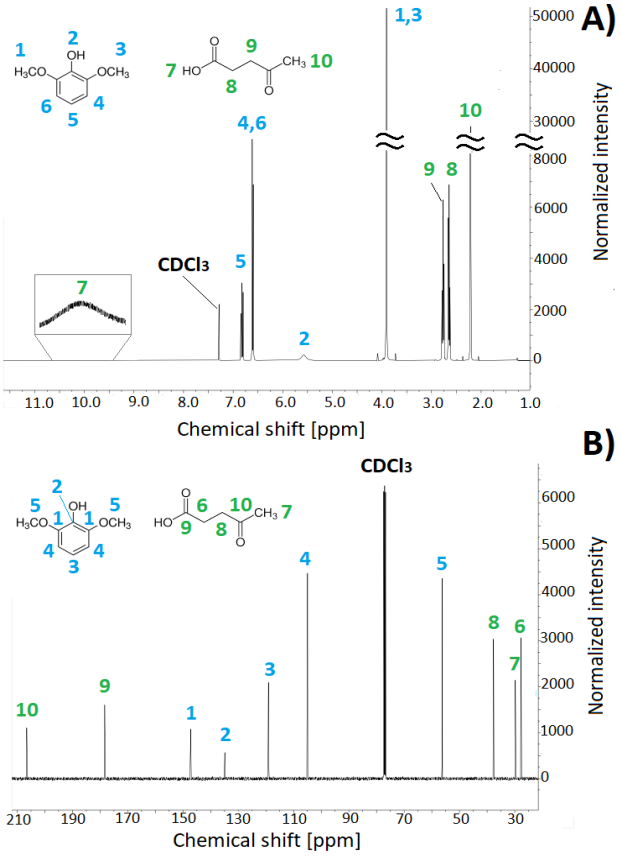


Figure 2 A) $^{1}$H NMR spectra of Syr:Lev (1:1), B) $^{13}$C NMR spectra of Syr:Lev (1:1).

Similar results of chemical shifts were also obtained in Gu:Lev (1:1) spectrum. In which the H proton shifts of the -COOH group with respect to pure levulinic acid (δδ = 0.12 ppm) were shifts towards lower values. Additionally, in $^{1}$H NMR spectrum the lower value of H proton shift of the -OH group with respect to pure guiacol, were observed (Fig. S1). In Gu:Lev (1:1) spectrum the carbon chemical shifts (δδ) towards lower values of the C atom from the ketone group (Lev) (δδ = 0.14) and carbon atom connected to OH group (Gu) (δδ = 0.11 ppm) with respect to pure the pure components were obtained. This indicates that two hydrogen bonds between Gu and Lev were formed. In the DES-based on C:Lev (1:2) (Fig. S2) and C:Gu (1:1) (Fig. S3) also very similar proton and carbon chemical shifts (δδ) can be observed. In the C:Lev (1:2) proton chemical shifts towards lower values resulting from the connected the O atom from the ketone group (C) to the H atom from of the COOH group (Lev), while in C:Gu (1:1) the proton chemical shifts come from the connected the O atom from the ketone group (C) to the H atom from of the OH group (Gu). The results shifts were δδ = 0.10 ppm and δδ = 0.12 ppm, respectively. In addition, in C:Lev (1:2) the shifts towards lower values, which are results of the formation of hydrogen bonds among two COOH groups from two levulinic acid molecules, can be observed. The calculated shift was 0.11 ppm. The described proton chemical

shifts (δδ) affects towards lower values carbon chemical shifts both in the C=O group (C) and in the COOH groups (Lev) in the C:Lev (1:2). The observed shifts were δδ = 0.79 ppm and δδ=0.25 ppm, respectively. For the C:Gu (1:1) observed similar results. The values of carbon chemical shifts towards lower values both in the C=O group (C) and in the C-OH group (Gu)

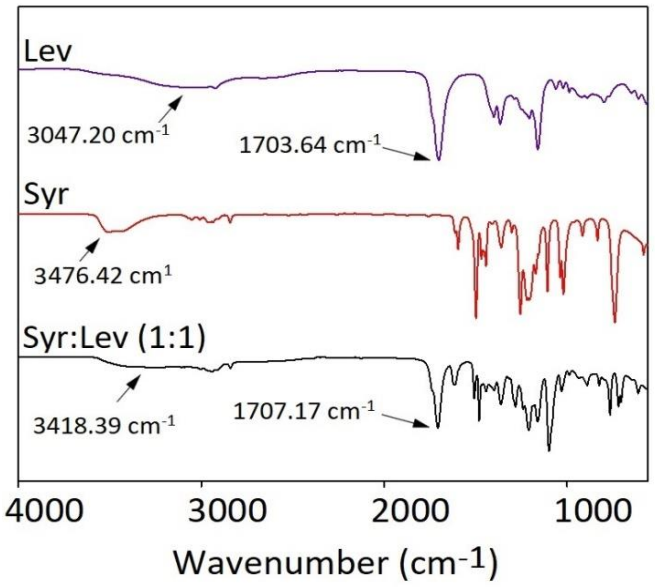


Figure 4 FT-IR spectrum of pure Lev, Syr, and Syr:Lev (1:1).

were δδ = 0.32 ppm and δδ = 0.05 ppm, respectively.

In the next part of the studies, Fourier transforms infrared spectroscopy (FTIR) was used to identify structures of new DESs and study the interaction between HBA and HBD in DES complexes. The FT-IR spectra of pure HBA and HBD components and the newly DESs created are shown in Fig. 4. As well known, DESs are created on the basis of specific intermolecular interactions (such as hydrogen bonds, dipole-dipole interactions, or van der Waals forces) between HBA and HBD. The location of the bonds depends on the structure of the HBA and HBD. In the FT-IR spectra of Syr:Lev (1:1) the shift of the signal corresponding to the of –OH stretching bonds relative to pure HBD (syringol) towards lower wavenumbers can be observed (Fig. 4). The shift is caused by a hydrogen bond formation between syringol and levulinic acid [72]. In addition, the characteristic shift of the bands corresponding to stretching vibrations of the C=O group towards higher wavenumbers (from 1703.64 cm-1 to 1707.17 cm-1) relative to pure HBA (levulinic acid) [73], can be observed. Similar wavenumber shifts can be observed for the remaining DES (Fig. S4-S6).

**Theoretical studies on DESs formation**

Information from spectroscopic analysis are not unambiguous, and they only indicates of existing strong hydrogen bonds between HBA and HBD. However, they do not indicate the number of hydrogen bonds, their exact location and information on weaker interactions, i.e. electrostatic interactions in DESs structures. Therefore additional quantum mechanical calculation based on DFT analysis was used to gain an insight into the non-bonded interactions of all DESs at the atomic level.

The most possible and stable DESs complexes in the gas phase were geometry optimized at the B3LYP/6-311++G** level of theory. DESs structures after geometric optimization are presented in Fig. 5A and Fig. S7. The obtained results show that non-bonded interaction can be found between HBA and HBD, which can be identified as strong hydrogen bonds (H-bonds) because of the distances below 2.5 Å between atoms. In Syr:Lev (1:1), the distance between ketone group in Lev and hydroxyl group from Syr (=O···H–O) is 1.89 Å. In C:Gu (1:1) is 1.83 Å between ketone group in C and hydroxyl group from Gu (=O···H–O). In G:Lev (1:1), two H-bond existed between hydroxyl group from Gu and ketone group in Lev =O···H–O (1.85 Å), as well as between hydroxyl group from Lev and methoxy group from Gu O–H···O-$CH_3$ (1.83 Å). In C:Lev (1:2) also two hydrogen bonds can be identified because of the short distances between the ketone group from C and hydroxyl group from one of the Lev molecule (=O···H–O) and hydroxyl groups from two Lev molecules O–H···H–O.

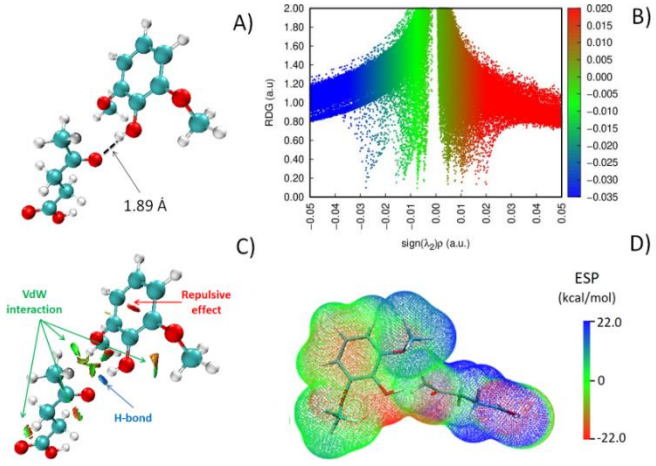


Figure 5 A) Structure of Syr:Lev (1:1) after geometric optimization; B) 2D plots of RDG versus the electron density multiplied by the sign of the second Hessian eigenvalue for Syr:Lev (1:1); C) Reduced density gradient (RDG) isosurfaces (s=0.5 a.u.) of Syr:Lev (1:1); D) Elecrostatic potential (ESP) mapped on electron total density with an isovalue 0.001 for Syr:Lev (1:1).

The classification and identification of all the non-covalent interactions (NCI) that exist between DESs components was prepared by means of reduced density gradient (RDG) analysis. The RDG analysis enables the identification of three types of interactions, i.e. H-bonds, van der Waals, and steric repulsion [49,74,75]. Fig. 5B and Fig. S8 show the 2D plots of reduced density gradient for Syr:Lev (1:1) and the rest of DESs, respectively. The results show that in DESs complexes, three type of NCI co-exist including H-bonds which corresponds to the negative sign of $(\lambda_2)\rho$ value (from −0.04 to −0.02 au); van der Waals interactions -0.01 au < sign $(\lambda_2)\rho$ < 0.01 au; and repulsive effect (sign $(\lambda_2)\rho$ < 0.02 au). The graphical interpretation of the obtained results are presented in Fig. 5C and Fig. S9, where blue areas represent strong attractive effects (H-bonds); red areas indicate strong repulsive interactions; green areas denote weaker NCI including van der Waals interaction. The results show that the only one

H-bond occur between HBA and HBD in Syr:Lev (1:1), and C:Gu (1:1). While, in C:Lev (1:2), and Gu:Lev (1:1), two hydrogen bonds can be observed in DES complexes. In all DES van der Waals interactions can be observed between HBA and HBD, and repulsive effect due to the presence of aromatic rings in DESs structures. The coexistence of all identified NCI between DES components corresponds to the decrease in MP in DES complexes in comparison to the melting points of the individual compounds [34,43].

In the next step of theoretical studies, the electrostatic potential analysis (EPA) was used to demonstrate the most possible and stable regions for the electrophilic attack, and predict how various geometries of DESs components could interact with each other. A comparison of the generated ESP maps for all studied DESs are presented in Fig. 5C and Fig. S10. The negative electrostatic potentials are appeared as red, the blue indicates positive potential, and green represent the closer to zero potentials. The results indicate that the electronegative areas are located around oxygen atom in all DESs structures. The positive regions are over hydrogen atoms in DESs molecules. Due to the fact that, the electronegative region is susceptible to an electrophilic attack and electropositive is region prone to nucleophilic attack, it can be predicted that the electronegative area of HBA will be close to the electropositive area of HBD during the DESs formation. All complexes presented in Fig. 5C and Fig. S10 confirms this prediction. For example, when Lev molecule interacts with Syr molecule, the red region located around oxygen atom is attracted to the blue region around hydrogen in hydroxyl group from Syr, forming hydrogen bond interactions. The same interaction behaviors were observed for the remaining DESs.

**Absorption of VOX compounds**

In order to systematically compare the absorption performance, the effect of several absorption factors including temperature, gas type, gas flow rate, inlet concentration, were studied.

**Effects of DES type on the absorption process**

The VOXs were absorbed in DES at 20°C and 10 kPa pressure. The initial concentration of individual VOX compounds were 0,5 mg/cm$^3$. The VOX removal efficiency was analyzed by gas chromatography after every 20 min time intervals. Fig. 6 presents VOX experimental breakthrough curves of four types of DESs. All experimental breakthrough curves could be divided into two parts. In the first part of the curves, the significantly increased outlet VOXs concentration with the increase in time of the process and further gradually reached the breakthrough point can be observed. In the next part of the curves, VOXs concentration reaches saturation, and no further changes in concentration are observed. The obtained shape of equilibrium curves is the result of the absorption law, which can be explained by the principle of gas–liquid equilibrium of the system. In the absorption process, simultaneously the mass

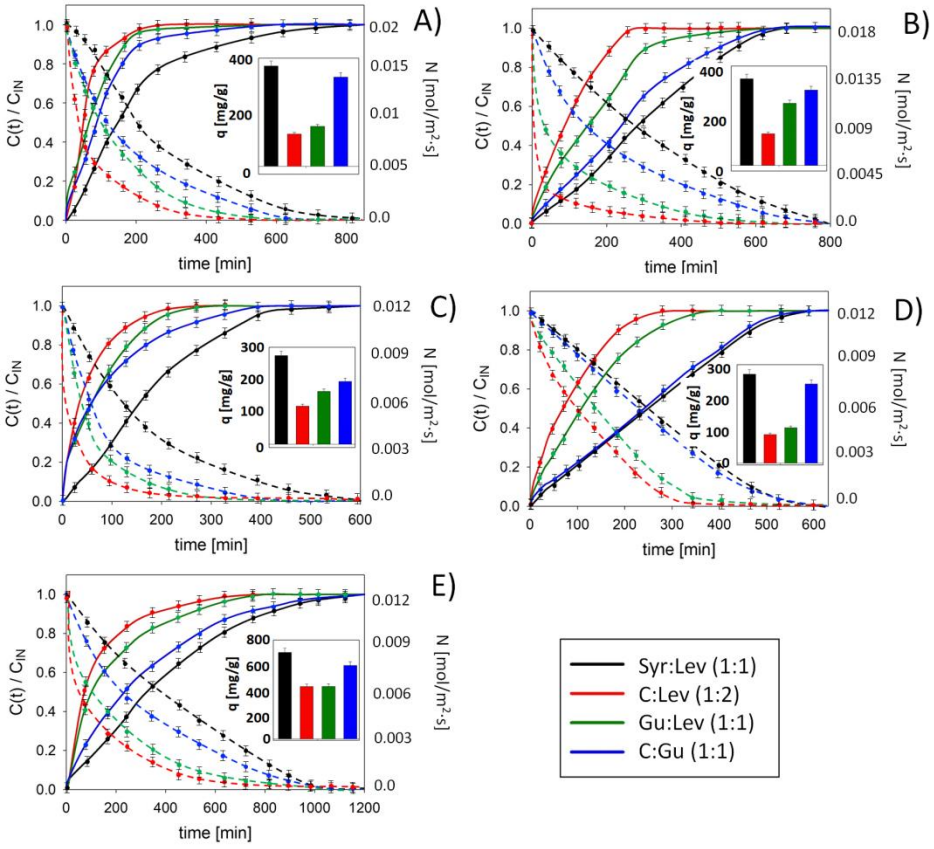


Figure 6 Experimental breakthrough curves (solid line) and absorption rate (dashed line) of a) DCM; b) CF; c) TCM; d) TCE; e) TCEtOH on different DESs (temperature 20 °C; inlet VOX concentration 0.5 mg/cm$^3$; gas flow 50 mL/min; matrix gas $N_2$).

transfer of VOX from biogas to DES, and from DES to the biogas stream occur. When the VOX concentration in DES reaches a certain ratio with the VOX concentration in the biogas stream, the rate of VOX mass transfer becomes equal to that of the desorption of VOX from DES (gas–liquid dynamic equilibrium).[76] The results indicate that the highest absorption capacity was observed for Syr:Lev (1:1) (Fig. 6). The absorption capacity for DCM, CF, TCM, TCE, and TCEtOH were 420 ± 22, 360 ± 16, 304 ± 11, 292 ± 8, and 661 ± 34 mg/g, respectively. Slightly lower absorption capacities were obtained for C:Gu (1:1). The absorption capacity were 365 ± 14, 320 ± 11, 275 ± 9, 266 ± 8, and 561 ± 18 mg/g for DCM, CF, TCM, TCE, and TCEtOH, respectively.

The obtained results indicate that the absorption capacities for the synthesized DES are higher compared to other absorbents and solid adsorbents. The absorption capacity of the developed DES is up to 100 times greater than that of ionic deep eutectic solvents based on quaternary ammonium salts (i.e. choline chloride, tetrabutylammonium bromide or tetrapropylammonium brmide). [51] Ionic liquids have slightly lower absorption capacities compared to the new DES.[77] However, their high price makes them almost impossible to use in industrial processes. Higher absorption capacity can be obtained for the metal organic framework UiO-66, however, as in the case of ILs, the unit price for 1 kg of adsorbent is 79207.2 €.[78] This makes the process completely uneconomical despite its high efficiency. The price of new DES varies depending on the components used to synthesize them. DESs price can vary from 24.02 € to 263.5 € per 1 kg. The price is lower than most of the absorbents and adsorbents described in the literature. The combination of price and high efficiency of VOX removal from biogas makes the new DESs have potential for industrial applications. The comparison of the available absorption and adsorption processes are presented in the Table S1.

Additionally, for all processes, the absorption rate was determined. As expected, the obtained results indicate that with the passage of time, a decrease in the absorption rate is observed. This is due to the decrease in the number of available DES active sites for VOX, which is associated with a reduction in the driving force of the absorption process (Fig. 6). [79] In addition, the absorption rate decrease due to the decrease in the difference between the concentration of impurities in the gas and in DES phase. The combination of absorption rate and absorption capacity enables a complete evaluation of the absorption process, which is very important from an economic and an industrial point of view. In Fig. 6, at the point of intersection of the absorption curve and absorption rate curve, the time during which the absorption process is very fast and effective can be determined. After this time is exceeded, the absorbent must be regenerated because the absorption process becomes ineffective and uneconomical. For Syr:Lev (1:1), the time for quick and effective absorption is 193 ± 8, 290 ± 11, 170 ± 5, 252 ± 9, 385 ± 19 min for DCM, CF, TCM, TCE and TCEtOH, respectively. It is in some cases 11 times longer compared to C: Lev (1: 2).

**Effects of temperature on the absorption process**

Under real conditions, the produced biogas is immediately introduced into the treatment system. Depending on the fermentation method used, the temperature of the raw biogas varies from 35 to 40 ° C, or from 50 to 55 ° C for the mesophilic and thermophilic method, respectively [80,81]. During designing a new biogas plant, an economic analysis should be made [22]. At this stage, it is necessary to decide whether it is more profitable to apply additional biogas cooling before purification, or to regenerate or replace the absorbent more often. Therefore, it is very important to know how the increase in temperature affects the absorption capacity. The studies of the influence of temperature on VOX absorption efficiency were carried on intervals of 20°C, 30°C, 40°C, 50°C, and 60°C. As expected, the capacity of VOX decreases by almost 50% with increasing temperature (Fig. 7A and S11). This phenomenon can be explained by the exothermic nature of the process for the absorption of VOX in DES. Higher temperature weakens the interactions between DES and VOX, allowing the VOX to leave the absorbent because of increased kinetic energy.[82]

**Effects of gas flow and gas type on the absorption process**

In the next part of the studies, the effect of gas flow rate in the range of 25 – 75 mL/min was determined (Fig. 7B and S12). The obtained results indicate that in the range tested, the biogas flow rate has only a minor effect on the absorption capacity of VOX. As the flow rate increases from 25 to 75 mL/min, the Syr:Lev (1:1) absorption capacity of DCM, CF, TCM, TCE, and TCEtOH is slightly reduced from 426 ± 20 to 417 ± 19 mg/g, from 356 ± 17 to 349 ± 16 mg/g, from 305 ± 14 to 293 ± 11 mg/g, from 284 ± 14 to 278 ± 14 mg/g, and from 664 ± 22 to 661 ± 24 mg/g, respectively. Similar results were obtained for other DESs. This phenomenon can be explained by the fact that as the gas flow rate increases, the contact time of the biogas stream contained VOXs with the DES is reduced, which adversely affects the VOXs absorption process.[43] On the other hand, in industrial processes, the contaminated gas flow should be as high as possible in order to obtain a large volume of clean gas in the shortest time. Therefore, 75 mL min was considered the optimal flowrate.

In the real biogas stream, the concentration of methane and carbon dioxide ranging from 50 to 80% v/v, and from 15 to 45 % v/v. Typically the concentration of water vapor and nitrogen does not exceed 2% v/v. Therefore in the studies, in order to recreate the real biogas stream under laboratory conditions, the type of matrix gas including pure nitrogen, pure methane or mixture of gases $CH_4$:$CO_2$:$N_2$:$H_2O$ in 81:15:2:2, 66:30:2:2, and 51:45:2:2 v/v were tested. As expected nitrogen was not absorbed into DES due to its neutral character. Therefore the appearance of $N_2$ in the biogas stream do not effect on the VOX absorption efficiency. The use of methane reduced the absorption capacity of DES by an average of 0.7% compared to nitrogen (Fig. 7B and S12). This is probably due to the absorption of $CH_4$ by Syr:Lev (1:1). Absorbed $CH_4$ can bind to Syr:Lev (1:1), thus blocking active sites. However, due to the only slight reduction in the DES absorption capacity, it can be

concluded that the methane is only absorbed to a small extent. Which is beneficial for the production of clean bio-methane from contaminated biogas. Based on the previous studies, methane is absorbed in most DES at a concentration of about 5%.[43,83,84] In commercial technologies (i.e. water scrubber, amine scrubber, membrane technologies), methane losses ranging from 0.04 to 1.97% v / v are observed.[57] Therefore, it can be concluded that the new method based on DES is within the acceptable range.

The substances that can negatively affect the removal of VOX from biogas are water and carbon dioxide. Both $H_2O$ and $CO_2$ have active oxygen atoms in their structures, which can form strong hydrogen bonds with DES. The strong interaction of carbon dioxide and water with DES removes them from the gas phase. This is a positive development from the biogas purification point of view. However, it can also block the DES active sites to which VOX compounds are attached. As a rule, water is present in low concentrations in biogas, so its importance is lower than $CO_2$. In the real absorption process, the biogas is dried before being introduction into the absorption column. The drying of the biogas takes place during its cooling. Part of the water vapor separates out as condensate. This process also removes other undesirable components, water-soluble gases and aerosols. Gas transmission installations include condensate containers in which the water vapor condensate formed during cooling is collected. [85] As expected, the obtained results indicate that as the concentration of $CO_2$ in the biogas increases from 0 to 45% v/v, the absorption efficiency of most VOX decreases (Fig. 7C). A reduction in the absorptive capacity and rate of VOX can be observed and, consequently, a reduction in the effective VOX absorption time from 138 to 89 min. However, during VOX absorption from biogas containing 30 and 45% v/v $CO_2$, no significant difference in VOX absorption capacity and rate was observed. This is most likely due to the limited solubility of $CO_2$ in Syr: Lev (1:1). Very similar results were obtained for CF, TCE and TCM (Fig. S13). Unexpected results were obtained for TCEtOH. With the increase in the concentration of carbon dioxide in the biogas at the inlet to the column, the absorption efficiency increased (absorption rate and capacity). The effective absorption time increase from 640 to 1200 min. This is probably because $CO_2$ molecules that attach to DES create additional active sites to which TCEtOH can attach. The -OH group from TCEtOH can both form strong hydrogen bonds with DES and $CO_2$. However, the increase in $CO_2$ concentration from 30 to 45% v/v did not increase the absorption efficiency due to the limited solubility of $CO_2$ in DES.

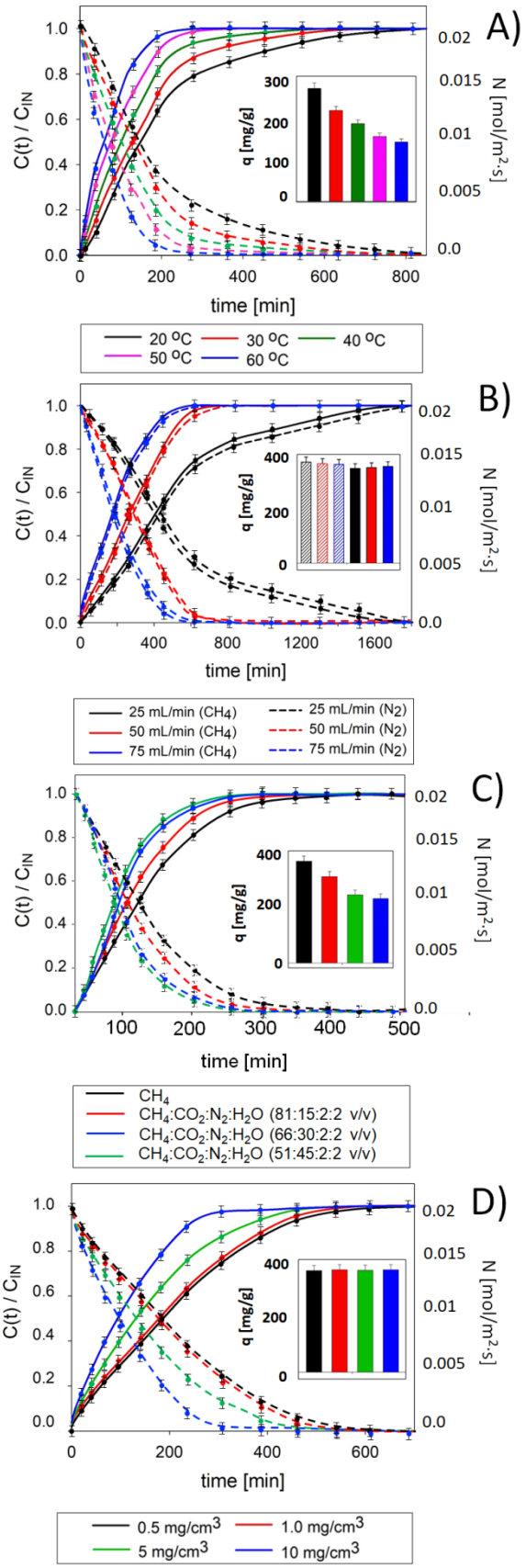


Figure 7 Experimental breakthrough curves of DCM at A) different temperatures for Syr:Lev (1:1) (inlet VOX concentration 0.5 mg/cm3; gas flow 50 mL/min; matrix gas N2); B) different gas flow rate for Syr:Lev (1:1) (inlet VOX concentration 0.5 mg/cm3; temperature 20°C); C) different gas matrix for Syr:Lev (1:1) (inlet VOX concentration 0.5 mg/cm3; temperature 20°C); D) initial concentration for Syr:Lev (1:1) (gas flow 50 mL/min; temperature 20°C).

**Effects of VOXs type and their concentration on the absorption process**

The average VOXs concentration in real biogas mostly depends on the kind of materials used for bio-methane production. Due to the fact that VOXs concentrations are very variable, in the next part of the work, the influence of VOXs concentrations in the range of 0.5 – 10 mg/cm³ on the absorption process was studied. As expected the obtained results indicate that the initial concentration of VOXs has only an impact on the saturation time, however, it has no effect on the total DES absorption capacity (Fig. 7D and S14). Increasing VOXs concentration in biogas stream from 0.5 to 1 mg/cm³ did not cause any significant differences in saturation time. However, a further increase in the concentration to 10 mg/m³ results in a noticeable reduction in the absorbent saturation time from 612.1 to 211.8 min for DCM (Fig. 7D). For the other DESs, the same behavior can be observed (Fig. S14). This indicates that with an increase of VOXs concentrations from 0.5 to 10.0 mg/m³, the VOXs removal efficiency gradually decreases. This is due to the fact that increasing VOXs concentration increases the molar ratio of VOXs/DES, resulting in decreased absorption efficiency of VOXs.

The selectivity of individual VOX was determined by comparing the VOX absorption to the sum of all VOX absorption in DES. The obtained results indicate that TCEtOH is characterized by the highest selectivity (TCEtOH/ΣVOX = 0.32). Slightly lower values were obtained for DCM (0.21) and CF (0.18), and the lowest values for TCM (0.15) and TCE (0.14). The high selectivity of TCEtOH is due to the presence of the -OH group in the structure, which can form strong hydrogen bonds with DES components. The remaining VOX do not have active groups in their structures, therefore they will interact with DES only with weaker electrostatic bonds. On the basis of the obtained results, it can be concluded that with the increase in the content of chlorine atoms in the VOX structures, the electrostatic interactions weaken. For a detailed explanation, see Mechanism of absorption.

**Regeneration of DES**

From an industrial and economic point of view, absorbents regeneration is a very important factor due to the fact that multiple uses of absorbent significantly reduces the cost of the process [22]. "The obtained results as expected indicate that desorption efficiency increases with increasing temperature from 20 to 100°C. The highest desorption efficiency of VOXs was obtained at 100°C. At 100°C, the complete desorption time was 60 minutes. However, at 80°C, the time necessary for the desorption increased to 180 minutes. Below 80 °C, even after 700 minutes of the process, 100% VOX removal from DES was not achieved. The similar results were obtained in previous studies.[86] The effect of temperature on VOXs desorption in Syr:Lev (1:1) is presented in Fig. 8. As shown in Fig. 8A and S15, absorption capacity is only slightly lost after ten cycles (absorption- desorption). In addition, a comparison of the FT-IR spectra of fresh DES and DES after ten cycles of absorption-desorption shows no additional peaks or band shifts Fig. 8B. This indicates that Sy:Lev (1:1) is stable during multiple cycles can be reused as VOXs absorbent. In similar conditions, ILs based on 1-butyl-3-methylimidazolium thiocyanate [Bmim][SCN] show only up to five effective DCM absorption-desorption cycles.[77]

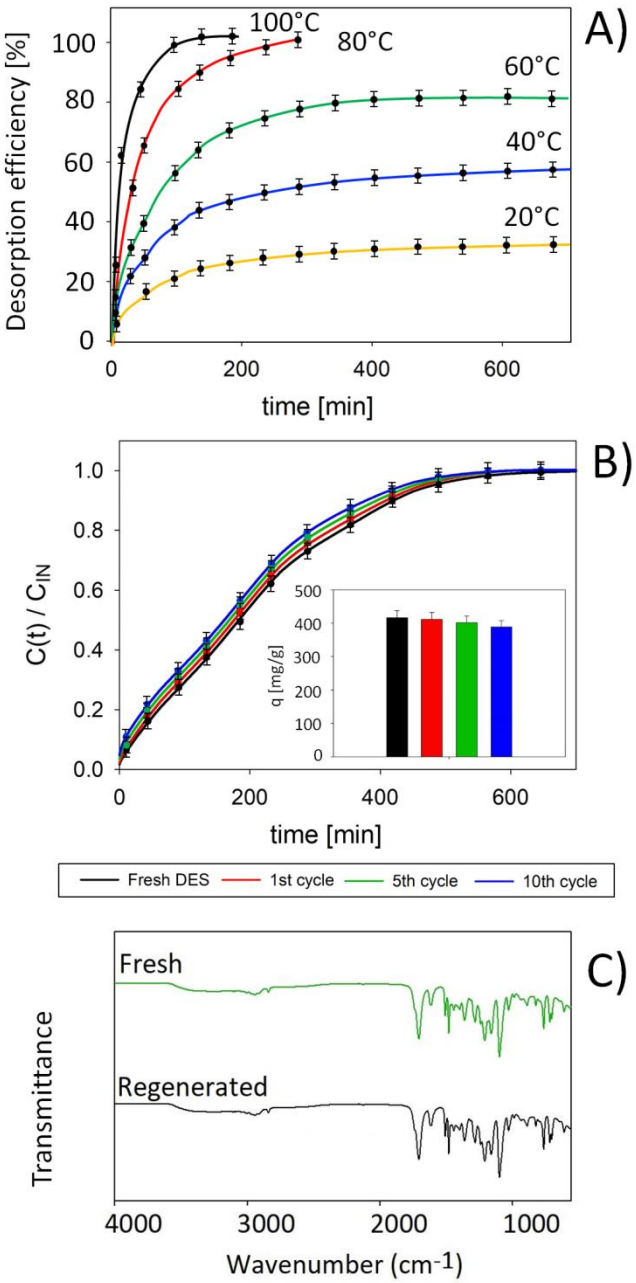


Figure 8 VOXs absorption/desorption cycles of Syr:Lev (1:1): A) Effect of temperature on Syr:Lev (1:1) desorption; B) Experimental breakthrough curves of DCM after absorption/desorption cycles (gas flow 70 mL/min; matrix gas $N_2$; temperature 20°C); C) FT-IR spectrum of fresh Syr:Lev (1:1) and regenerated DES.

**Mechanism of absorption**

In order to explain the absorption mechanism, DESs - VOX complexes were characterized by FT-IR, as well as quantum mechanical calculations. The FT-IR spectra of Syr:Lev (1:1) before and after absorption of selected volatile organic halogens are present in Fig. 9A and S16. The comparison of the spectrum of pure Syr:Lev (1:1) with Syr:Lev (1:1) after TCEtOH absorption show the shift of the -OH bands towards higher values from 3418.39 $cm^{-1}$ to 3446.81 $cm^{-1}$, as well as the carbonyl group towards higher values from 1707.17 $cm^{-1}$ to 1712.82 $cm^{-1}$ (Fig. S15). The increase in the intensity of the -OH and C=O band confirms the formation of a hydrogen bond between Syr:Lev (1:1), and the TCEtOH.[87] In addition, in the DES spectrum after absorption TCEtOH in the range 1097.76-714.13 $cm^{-1}$ the vibrations which should be assigned to the C-O stretching bond (1086.64 $cm^{-1}$), C-Cl bond (807.95 $cm^{-1}$), and C-H bending bond (709.96 $cm^{-1}$) present in pure TCEtOH are visible, which confirms further interaction between Syr:Lev (1:1) and TCEtOH.[88] In the FT-IR spectra after the absorption of DCM, CF, TCM, and TCE (Fig. 9A and S16) one can notice a shift of the -OH group and the C=O group towards higher wavenumber values. The observed changes confirm that the absorption process may take place through the formation of weak hydrogen bonds between the COOH group (derived from Syr:Lev) and the chlorine atom (derived from VOX). Similar results can be observed for C:Lev (1:2), C:Gu (1:1), and G:Lev (1:1) (Fig. S17-S19).

The results of calculation studies indicate that non-bonded interaction exists between both components of DESs and all VOXs (Fig. 9B and S20-S23). Theoretically, chloride atoms of VOXs can interact with hydroxyl groups of DES (C-Cl···HO), or the C-H group can interact with carbonyl (C-H···O=) or hydroxyl groups of DESs (C-H···OH) forming weak hydrogen bonds.[89,90] However, C-H and Cl-C groups are a weak donor and very weak acceptor, respectively. These groups can form only weak hydrogen bonds. In the optimized complexes of Syr:Lev (1:1) –

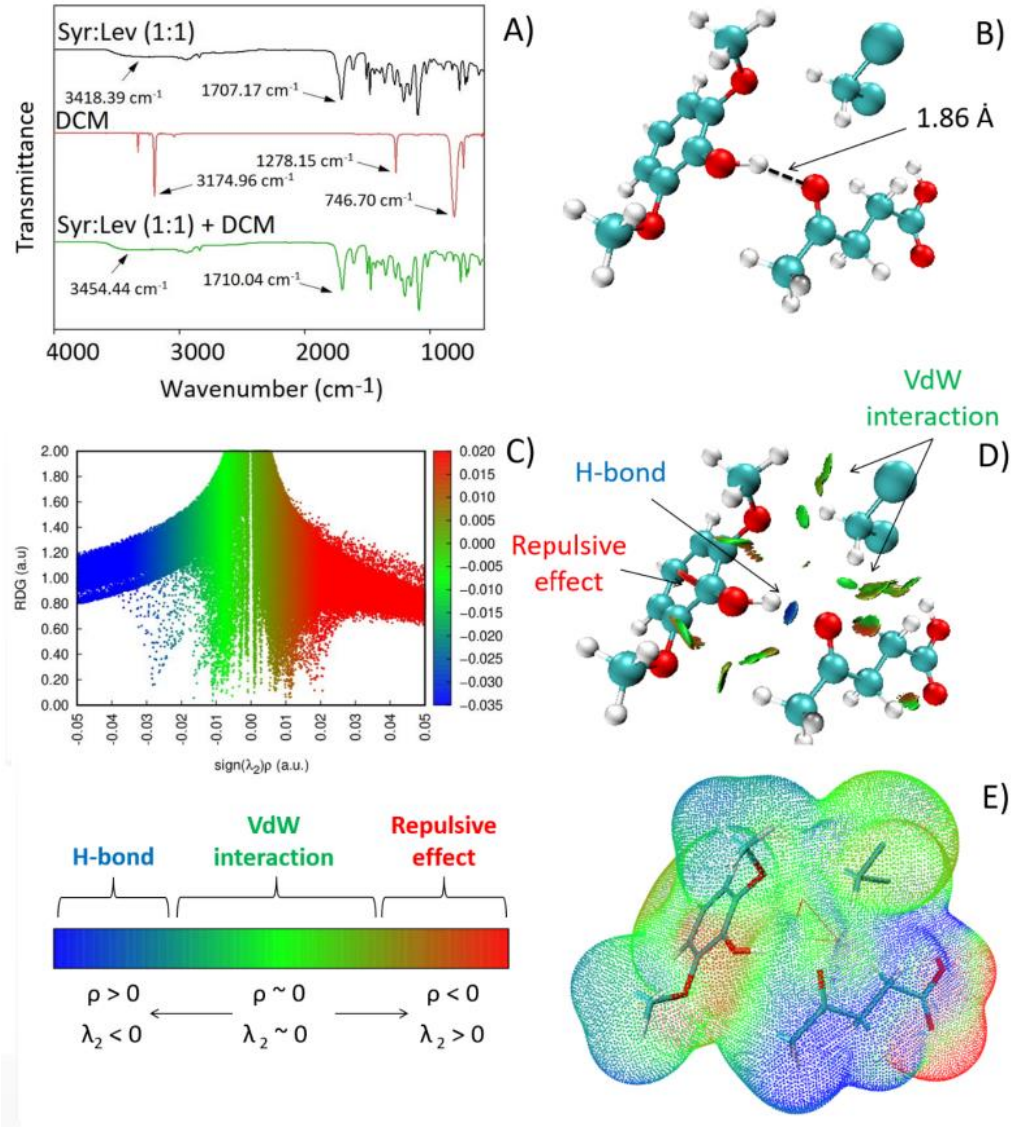


Figure 9 A) FT-IR spectra of pure Syr:Lev (1:1), pure DCM, and Syr:Lev (1:1) – DCM complex; B) Syr:Lev (1:1) – DCM structure after geometric optimization; C) 2D plots of RDG versus the electron density multiplied by the sign of the second Hessian eigenvalue for Syr:Lev (1:1) – DCM; D) Reduced density gradient (RDG) isosurfaces (s=0.5 a.u.) of Syr:Lev (1:1) – DCM; E) Electrostatic potential (ESP) mapped on electron total density with an isovalue 0.001 for Syr:Lev (1:1) – DCM.

DCM, Syr:Lev (1:1) – CF, Syr:Lev (1:1) – TCM, and Syr:Lev (1:1) – TCE, the distances between hydroxyl groups of DES components
and chloride atoms of VOXs are higher than 2.5 Å, which indicates the absence of hydrogen bonds, and another interaction must play a major role in removing VOXs from the biogas stream. A similar phenomenon was observed for the remaining DES. Only in Syr:Lev (1:1) – TCEtOH complex, two H-bonds exist between the hydroxyl group of TCEtOH and hydroxyl groups of Syr and Lev -OH···HO (1.79 and 1.8 Å), which may affect the higher absorption of TCEtOH compared to other VOX. On the other hand, it can be observed that when the TCEtOH molecule is attached to Syr:Lev (1:1), H-bond between Syr and Lev in DES becomes weaker. Similar behavior can be observed in Gu:Lev (1:1) -TCEtOH complex, in which one of the existed hydrogen bonds between Gu and Lev has been broken, and in its place an additional hydrogen bond between the carbonyl group of Lev and hydroxyl group of TCEtOH =O···HO (1.94 Å) was formed. In C:Lev (1:2) – TCEtOH and C:Gu (1:1) – TCEtOH complexes, additional hydrogen bonds were formed between DESs and TCEtOH, and existing hydrogen bonds between DES components were not weakened or broken, which indicate the high stability of DESs during the absorption process. The obtained results of reduced density gradient analysis show that van der Waals interactions occur in all DES-VOX complexes, with the exception of DES-TCEtOH complexes in which both hydrogen bonding and van der Waals interactions are coexisted (Fig. 9CD and S24-S31). The green surfaces of the van der Waals interaction increase following the order of C:Lev (1:2) < G:Lev (1:1) < C:Gu (1:1) < Syr:Lev (1:1), which is in line with the results obtained for the absorption processes. The obtained results show that the non-covalent interactions (mainly van der Waals) are the main driving force for DCM, CF, TCM, and TCE removal from gas streams. While coexisting H-bonds and electrostatic interactions are responsible for the effective removal of TCEtOH.

The results of the electrostatic potential analysis of the VOXs compounds indicate that the electropositive areas are located around hydrogen atoms in DCM, CF, and TCEtOH. The electronegative areas are located around the oxygen and chloride atoms in VOX, and the neutral regions are located close to carbon atoms (Fig. 9E and S32-S35). When VOXs (with exception of TCEtOH) interacts with DESs, the electropositive region located around hydrogen atoms in all DESs is attracted to the electronegative area located close to chloride atoms in VOX. While, when TCEtOH interacts with DESs, the electropositive region located around the H atom in the hydroxyl group is attracted to the electronegative region located close to oxygen in the hydroxyl group, forming the H-bond interaction. The obtained interaction energy (ΔEint) between all studied DESs and VOXs are presented in Table 1. The more negative values of interaction energies indicate stronger interactions between DES and VOX. It can be observed that, the $\Delta E_{int}$ followed a similar trend to that of the experimental absorption capacity of VOX (C:Lev (1:2) > G:Lev (1:1) > C:Gu (1:1) > Syr:Lev (1:1)). Moreover, taking into account the individual VOX, the interaction energy can be ranked as follows TCE ~ TCM > DCM > TCEtOH, which is also in line with the results obtained experimentally.

Table 1 Interaction energies between DES and VOX.

| DES | Interaction energy [kcal/mol] | | | | |
|---|---|---|---|---|---|
| | DCM | CF | TCM | TCEtOH | TCE |
| C:Lev (1:2) | -6.7 | -6.1 | -2.0 | -10.5 | -1.8 |
| C:Gu (1:1) | -7.0 | -5.3 | -2.7 | -11.5 | -2.5 |
| Gu:Lev (1:1) | -0.8 | -0.4 | -0.3 | -1.9 | -0.2 |
| Syr:Lev (1:1) | -5.9 | -5.3 | -2.6 | -8.2 | -1.4 |

## Conclusions

New deep eutectic solvents composed of natural ingredients were successfully applied for the removal of volatile organochlorine compounds from the biogas stream in the absorption process. The influence of several absorption parameters i.e. type of DES, gas flowrate, kind of matrix gas, temperature, and initial concentrations of VOXs on absorption process were studied. It was found that the Syr:Lev (1:1) has the highest absorption capacity of VOXs, at 20°C. The other parameters, i.e. the initial concentration of VOXs and the gas flow, only affect the extension or reduction of the DES saturation time. However, they do not significantly affect the DES absorption capacity. In optimal conditions, the absorption capacity of DCM, CF, TCM, TCE, and TCEtOH were 304, 420, 360, 292, and 661 mg/g, respectively. The obtained results of the absorption capacity for DCM are higher by about 98 mg/g compared to the results obtained with the use of ILs based on [Bmim][SCN].[77] After the absorption process, Syr:Lev (1:1) was successfully regenerated by means of nitrogen barbotage at 100°C in one hour. The obtained results demonstrated that the absorption capacities of Syr:Lev (1:1) did not change after ten absorption-desorption cycles which confirms the stable reusable capacity. The theoretical and experimental studies on the mechanism of DESs formation and VOX absorption indicate that both h-bonding and van der Waals interaction between DES components contributes to stable eutectic mixtures formation. In addition, depending on the type of VOXs, only van der Waals or both hydrogen bonds and van der Waals interactions are the main driving forces for the removal of VOXs from model biogas. Therefore, the proposed procedure based on DESs has great potential for the purification of the real biogas streams, and is in line with the green engineering strategy as well as the European Union's strategy for obtaining renewable energy.

## Author Contributions

**Patrycja Makoś-Chełstowska**: Conceptualization, Data curation, Funding acquisition, Formal Analysis, Investigation, Methodology, Supervision, Writing – original draft, Writing – review & editing. **Edyta Słupek**: Conceptualization, Data

curation, Investigation, Methodology, Writing – original draft. **Jacek Gębicki**: Writing – review & editing.

## Conflicts of interest

There are no conflicts to declare.

## Acknowledgements

This work was supported by Gdańsk University of Technology under the Argentum Triggering Research Grants—EIRU program Grant (No. DEC-34/2020/IDUB/I.3.3).

## References

1 B. Stürmer, D. Leiers, V. Anspach, E. Brügging, D. Scharfy and T. Wissel, *Renew. Energy*, 2021, **164**, 171–182.
2 T. Tomić and D. R. Schneider, *Renew. Sustain. Energy Rev.*, 2018, **98**, 268–287.
3 L. Lijó, S. González-García, J. Bacenetti and M. T. Moreira, *Energy*, 2017, **137**, 1130–1143.
4 S. Rasi, J. Läntelä and J. Rintala, *Energy Convers. Manag.*, 2011, **52**, 3369–3375.
5 G. Piechota, B. Igliński and R. Buczkowski, *Energy Convers. Manag.*, 2013, **68**, 219–226.
6 N. Scarlat, J. F. Dallemand and F. Fahl, *Renew. Energy*, 2018, **129**, 457–472.
7 J. I. Salazar Gómez, H. Lohmann and J. Krassowski, *Chemosphere*, 2016, **153**, 48–57.
8 S. Rasi, A. Veijanen and J. Rintala, *Energy*, 2007, **32**, 1375–1380.
9 I. A. Arkharov, E. N. Simakova and E. S. Navasardyan, *Chem. Pet. Eng.*, 2016, **52**, 547–551.
10 A. Jaffrin, N. Bentounes, A. M. Joan and S. Makhlouf, *Biosyst. Eng.*, 2003, **86**, 113–123.
11 R. J. Spiegel and J. L. Preston, *Energy*, 2003, **28**, 397–409.
12 H. C. Shin, J. W. Park, K. Park and H. C. Song, *Environ. Pollut.*, 2002, **119**, 227–236.
13 F. Dincer, M. Odabasi and A. Muezzinoglu, *J. Chromatogr. A*, 2006, **1122**, 222–229.
14 B. V. Nielsen, S. Maneein, M. D. Mahmud Al Farid and J. J. Milledge, *Fermentation*, , DOI:10.3390/FERMENTATION6030085.
15 A. Buekens and H. Huang, *J. Hazard. Mater.*, 1998, **62**, 1–33.
16 O. W. Awe, Y. Zhao, A. Nzihou, D. P. Minh and N. Lyczko, *Waste and Biomass Valorization*, 2017, **8**, 267–283.
17 S. Rasi, J. Läntelä, A. Veijanen and J. Rintala, *Waste Manag.*, 2008, **28**, 1528–1534.
18 J. Lemus, M. Martin-Martinez, J. Palomar, L. Gomez-Sainero, M. A. Gilarranz and J. J. Rodriguez, *Chem. Eng. J.*, 2012, **211**–**212**, 246–254.
19 M. Abtahi, K. Naddafi, A. Mesdaghinia, K. Yaghmaeian, R. Nabizadeh, N. Jaafarzadeh, N. Rastkari, S. Nazmara and R. Saeedi, *J. Environ. Heal. Sci. Eng.*, 2014, **12**, 1–7.
20 R. Guo, S. Lv, T. Liao, F. Xi, J. Zhang, X. Zuo, X. Cao, Z. Feng and Y. Zhang, *Resour. Conserv. Recycl.*, 2020, **153**, 104580.
21 G. Orsatti, F. Quatraro and M. Pezzoni, *Res. Policy*, 2020, **49**, 103919.
22 E. Słupek, P. Makoś and J. Gębicki, *Energies*, 2020, **13**, 3379.
23 I. Angelidaki, L. Xie, G. Luo, Y. Zhang, H. Oechsner, A. Lemmer, R. Munoz and P. G. Kougias, *Biofuels Altern. Feed. Convers. Process. Prod. Liq. Gaseous Biofuels*, 2019, 817–843.
24 E. Ryckebosch, M. Drouillon and H. Vervaeren, *Biomass and Bioenergy*, 2011, **35**, 1633–1645.
25 Y. Xiao, H. Yuan, Y. Pang, S. Chen, B. Zhu, D. Zou, J. Ma, L. Yu and X. Li, *Chinese J. Chem. Eng.*, 2014, **22**, 950–953.
26 G. Darracq, A. Couvert, C. Couriol, A. Amrane, D. Thomas, E. Dumont, Y. Andres and P. Le Cloirec, *J. Chem. Technol. Biotechnol.*, 2010, **85**, 309–313.
27 G. F. Freeguard and R. Stock, *Trans. Faraday Soc.*, 1963, **59**, 1655–1662.
28 D. L. Feldheim, S. M. Hendrickson, M. Krejcik, C. M. Elliott and C. A. Foss, *J. Phys. Chem.*, 1995, **99**, 3288–3293.
29 A.-S. Rodriguez Castillo, P.-F. Biard, S. Guihéneuf, L. Paquin, A. Amrane and A. Couvert, *Chem. Eng. J.*, 2019, **360**, 1416–1426.
30 S. N. Turosung and B. Ghosh, *Int. J. Petrochemistry Res.*, 2017, **1**, 50–60.
31 A. Romero, A., Santos, A., Tojo, J. & Rodríguez, *J. Hazard. Mater.*, 2008, **151**, 268–273.
32 K. Häckl and W. Kunz, *Comptes Rendus Chim.*, 2018, **21**, 572–580.
33 T. P. Thuy Pham, C. W. Cho and Y. S. Yun, *Water Res.*, 2010, **44**, 352–372.
34 P. Makoś, E. Słupek and J. Gębicki, *J. Mol. Liq.*, 2020, **308**, 113101–113112.
35 P. Makoś, A. Fernandes, A. Przyjazny and G. Boczkaj, *J. Chromatogr. A*, , DOI:10.1016/j.chroma.2018.04.054.
36 P. Makoś and G. Boczkaj, *J. Mol. Liq.*, 2019, **296**, 111916–111927.
37 P. Makoś, A. Przyjazny and G. Boczkaj, *J. Chromatogr. A*, , DOI:10.1016/j.chroma.2018.07.070.
38 P. Makoś, E. Słupek and J. Gębicki, *Microchem. J.*, , DOI:10.1016/j.microc.2019.104384.
39 F.-Y. Zhong, K. Huang and H.-L. Peng, *J. Chem. Thermodyn.*, 2019, **129**, 5–11.
40 T. Aissaoui, I. M. AlNashef and Y. Benguerba, *J. Nat. Gas Sci. Eng.*, 2016, **30**, 571–577.
41 H. Wu, M. Shen, X. Chen, G. Yu, A. A. Abdeltawab and S. M. Yakout, *Sep. Purif. Technol.*, 2019, **224**, 281–289.
42 Y. Zhang, X. Ji and X. Lu, *Renew. Sustain. Energy Rev.*, 2018, **97**, 436–455.
43 E. Słupek and P. Makoś, *Sustainability*, 2020, **12**, 1619–1635.
44 E. Słupek, P. Makoś and J. Gębicki, *Arch. Environ. Prot.*, 2020, **46**, 41–46.
45 P. Makoś, E. Słupek and A. Małachowska, *Materials (Basel).*, 2020, **13**, 1894.
46 L. F. Zubeir, D. J. G. P. Van Osch, M. A. A. Rocha, F. Banat and M. C. Kroon, *J. Chem. Eng. Data*, 2018, **63**, 913–919.

47 H. Wu, M. Shen, X. Chen, G. Yu, A. A. Abdeltawab and S. M. Yakout, *Sep. Purif. Technol.*, 2019, **224**, 281–289.

48 Y. Chen, D. Yu, W. Chen, L. Fu and T. Mu, *Phys. Chem. Chem. Phys.*, 2019, **21**, 2601–2610.

49 M. Atilhan, T. Altamash and S. Aparicio, *Molecules*, 2019, **24**, 1–18.

50 E. Słupek, P. Makoś-Chełstowska and J. Gębicki, *Materials (Basel).*, 2021, **14**, 1–20.

51 E. Moura, L., Moufawad, T., Ferreira, M., Bricout, H., Tilloy, S., Monflier and S. Costa Gomes, M.F., Landy, D., Fourmentin, *Environ. Chem. Lett.*, 2017, **15**, 747–753.

52 R. Chromá, M. Vilková, I. Shepa, P. Makoś-Chełstowska and V. Andruch, *J. Mol. Liq.*, 2021, **330**, 115617.

53 R. Chromá, M. Vilková, I. Shepa, P. Makoś-Chełstowska and V. Andruch, *J. Mol. Liq.*, 2021, **330**, 115617.

54 V. Migliorati, F. Sessa and P. D'Angelo, *Chem. Phys. Lett. X*, 2019, **2**, 100001.

55 Z. Naseem, R. A. Shehzad, A. Ihsan, J. Iqbal, M. Zahid, A. Pervaiz and G. Sarwari, *Chem. Phys. Lett.*, 2021, **769**, 138427.

56 S. Khodaverdian, B. Dabirmanesh, A. Heydari, E. Dashtban-moghadam, K. Khajeh and F. Ghazi, *Int. J. Biol. Macromol.*, 2018, **107**, 2574–2579.

57 T. Kvist and N. Aryal, *Waste Manag.*, 2019, **87**, 295–300.

58 J. R. Bastidas-Oyanedel, F. Bonk, M. H. Thomsen and J. E. Schmidt, *Rev. Environ. Sci. Biotechnol.*, 2015, **14**, 473–498.

59 J. M. T. Vasconcelos, J. M. L. Rodrigues, S. C. P. Orvalho, S. S. Alves, R. L. Mendes and A. Reis, *Chem. Eng. Sci.*, 2003, **58**, 1431–1440.

60 S. Adams, P. De Castro, P. Echenique, J. Estrada, M. D. Hanwell, P. Murray-Rust, P. Sherwood, J. Thomas and J. Townsend, *J. Cheminform.*, 2011, **3**, 38.

61 F. Neese, *Wiley Interdiscip. Rev. Comput. Mol. Sci.*, 2012, **2**, 73–78.

62 S. Grimme, J. Antony, S. Ehrlich and H. Krieg, *J. Chem. Phys.*, , DOI:10.1063/1.3382344.

63 A. Gutiérrez, M. Atilhan and S. Aparicio, *Phys. Chem. Chem. Phys.*, 2018, **20**, 27464–27473.

64 T. Altamash, A. I. Amhamed, S. Aparicio and M. Atilhan, *Ind. Eng. Chem. Res.*, 2019, **58**, 8097–8111.

65 S. Simon, M. Duran and J. J. Dannenberg, *J. Chem. Phys.*, 1996, **105**, 11024–11031.

66 T. Lu and F. Chen, *J. Comput. Chem.*, 2012, **33**, 580–592.

67 T. Lu and F. Chen, *J. Mol. Graph. Model.*, 2012, **38**, 314–323.

68 E. R. Johnson, S. Keinan, P. Mori-Sánchez, J. Contreras-García, A. J. Cohen and W. Yang, *J. Am. Chem. Soc.*, 2010, **132**, 6498–6506.

69 W. Humphrey, A. Dalke and K. Schulten, *J. Mol. Graph.*, 1996, **14**, 33–38.

70 A. Hayyan, F. S. Mjalli, I. M. Alnashef, T. Al-Wahaibi, Y. M. Al-Wahaibi and M. A. Hashim, *Thermochim. Acta*, 2012, **541**, 70–75.

71 R. Haghbakhsh, K. Parvaneh, S. Raeissi and A. Shariati, *Fluid Phase Equilib.*, 2018, **470**, 193–202.

72 N. F. Gajardo-Parra, M. J. Lubben, J. M. Winnert, Á. Leiva, J. F. Brennecke and R. I. Canales, *J. Chem. Thermodyn.*, 2019, **133**, 272–284.

73 B. D. Ribeiro, C. Florindo, L. C. Iff, M. A. Z. Coelho and I. M. Marrucho, *ACS Sustain. Chem. Eng.*, 2015, **3**, 2469–2477.

74 R. A. Boto, J. Contreras-García, J. Tierny and J. P. Piquemal, *Mol. Phys.*, 2016, **114**, 1406–1414.

75 G. Saleh, C. Gatti and L. Lo Presti, *Comput. Theor. Chem.*, 2012, **998**, 148–163.

76 X. Ma, M. Wu, S. Liu, J. Huang, B. Sun, Y. Zhou, Q. Zhu and H. Lu, *Chinese J. Chem. Eng.*, 2019, **27**, 2383–2389.

77 W. Wu, T. Li, H. Gao, D. Shang, W. Tu, B. Wang and X. Zhang, *Guocheng Gongcheng Xuebao/The Chinese J. Process Eng.*, 2019, **19**, 173–180.

78 Y. Zhou, L. Zhou, X. Zhang and Y. Chen, *Microporous Mesoporous Mater.*, 2016, **225**, 488–493.

79 H. Pashaei, A. Ghaemi and M. Nasiri, *RSC Adv.*, 2016, **6**, 108075–108092.

80 G. Tian, B. Yang, M. Dong, R. Zhu, F. Yin, X. Zhao, Y. Wang, W. Xiao, Q. Wang, W. Zhang and X. Cui, *Renew. Energy*, 2018, **123**, 15–25.

81 E. Słupek, P. Makoś, K. Kucharska and J. Gębicki, *Chem. Pap.*, , DOI:10.1007/s11696-019-01010-6.

82 J. Lemus, J. Bedia, C. Moya, N. Alonso-Morales, M. A. Gilarranz, J. Palomar and J. J. Rodriguez, *RSC Adv.*, 2016, **6**, 61650–61660.

83 C. H. Hsu, H. Chu and C. M. Cho, *J. Air Waste Manag. Assoc.*, 2003, **53**, 246–252.

84 Y. Guo, Z. Niu and W. Lin, *Energy Procedia*, 2011, **4**, 512–518.

85 M. Netušil and P. Ditl, *S. Gupta, Nat. Gas Extr. to End Use*, 2012, 3–22.

86 K. Zhang, Y. Hou, Y. Wang, K. Wang, S. Ren and W. Wu, *Energy and Fuels*, 2018, **32**, 7727–7733.

87 S. Zhu, H. Li, W. Zhu, W. Jiang, C. Wang, P. Wu, Q. Zhang and H. Li, *J. Mol. Graph. Model.*, 2016, **68**, 158–175.

88 R. Gautam, N. Kumar and J. G. Lynam, *J. Mol. Struct.*, 2020, **1222**, 128849.

89 W. Caminati, S. Melandri, A. Maris and P. Ottaviani, *Angew. Chemie - Int. Ed.*, 2006, **45**, 2438–2442.

90 P. I. Nagy, *J. Phys. Chem. A*, 2013, **117**, 2812–2826.